dynamics

MDPI

Article

The Mechanism of How a Cavity Affects the Fluctuating Pressure Measurement Results of a Static Pressure Probe

Chao Wang [1,2,*], Xingyou Yi [1], Jinlei Lv [1] and Qiang Peng [1,2,*]

[1] Facility Design and Instrumentation Insitute, China Aerodynamics Research and Development Center, Mianyang 621000, China; lv_jl@163.com (J.L.)
[2] State Key Laboratory of Aerodynamics, China Aerodynamics Research and Development Center, Mianyang 621000, China
* Correspondence: wangchao3@cardc.cn (C.W.); pengqiang401@163.com (Q.P.)

Abstract: A static pressure probe is a crucial tool for measuring static pressure fluctuations, and its internal cavity structure can significantly affect the accuracy of the data obtained. This study investigates the impact of the static pressure probe cavity on the frequency response characteristics of fluctuating pressure using both experimental and numerical simulations. The results are validated by comparing them with the behavior of a second-order system. Our findings indicate that the internal cavity of the static pressure probe acts as a second-order underdamped system. This system amplifies fluctuating pressure signals at frequencies below the characteristic frequency while attenuating those above it. The frequency response characteristics of the probe's cavity are similar to those of a Helmholtz resonator. Among various factors, the diameter of the pressure tap within the cavity has the most significant effect on the system's characteristic frequency and amplification ratio. By optimizing the design of the static pressure probe's cavity dimensions, the precision of fluctuating pressure data below the system's characteristic frequency can be improved. In the research, based on the Helmholtz resonance equation, we provide a semi-empirical formula for predicting the characteristic frequency of fluctuating pressure in a static pressure probe. Furthermore, by leveraging the mechanism of the static pressure probe's cavity as a second-order underdamped system, we propose a method for rapid and accurate calibration of the static pressure probe's fluctuating pressure measurements.

Keywords: static pressure probe; fluctuating pressure calibration; cavity structure; second-order underdamped system; frequency response characteristics

Academic Editor: Christos Volos

Received: 20 November 2024
Revised: 5 December 2024
Accepted: 9 December 2024
Published: 2 January 2025

Citation: Wang, C.; Yi, X.; Lv, J.; Peng, Q. The Mechanism of How a Cavity Affects the Fluctuating Pressure Measurement Results of a Static Pressure Probe. *Dynamics* **2025**, *5*, 1. https://doi.org/10.3390/dynamics5010001

1. Introduction

In the aerospace field, accurate measurement of noise (static pressure fluctuations) plays a crucial role in evaluating equipment performance and analyzing flow mechanisms. For instance, in supersonic flows, fluctuating static pressure is a fundamental and important physical quantity for characterizing turbulent flows. Background pressure disturbances, represented primarily by static pressure fluctuations, can significantly influence the development trends of physical phenomena such as boundary layer transition and shock wave boundary layer interactions [1–3]. Furthermore, static pressure probes serve as a reliable tool for measuring pressure fluctuations and are widely applied in fluid dynamics measurements and research, including compressors, turbine rotors, and supersonic flows. However, with the increasing demand for higher measurement accuracy, researchers have gradually realized that the internal cavity structure of static pressure probes can exert a non-negligible impact on the obtained pressure fluctuation data [4–7].

The static pressure probe features a cavity between the pressure tap and the fluctuating pressure sensor. This cavity, combined with airflow disturbances caused by the pressure tap, can interfere with and modify incoming pressure waves, thereby affecting the accuracy of pressure fluctuation measurements. The internal cavity structure of the static pressure probe exhibits geometric traits similar to that of a Helmholtz resonator. Previous studies have demonstrated that Helmholtz resonators possess a specific natural frequency. When the external excitation frequency approaches this natural frequency, it can induce a strong resonant response, amplifying signals within certain frequency bands while attenuating others [8–10].

Shirahama [11] and Toyoda [12] attributed the frequency response disturbances of static pressure probes to the compressibility of air within the probe's cavity. They attempted to adjust the cavity structure parameters of the static pressure probe to reduce measurement uncertainties and disturbances. Takuya [13] investigated the frequency response characteristics of static pressure probes in water and found that these characteristics were independent of the fluid's compressibility. To achieve more accurate measurements of static pressure fluctuations, researchers have endeavored to calibrate the frequency response of the measurement results. Kawata [14] derived static pressure fluctuation data from velocity and total pressure measurements using the unsteady Bernoulli equation. This method was experimentally validated for accuracy, but its highest measurable frequency was limited to 650 Hz. The accuracy of this approach at higher frequencies remains uncertain. Chaudhry [15] investigated the transfer function for probe frequency calibration and found that it strongly depends on the cavity's geometry. The lack of standardization in shape and size renders it challenging to compare results from other studies.

Additionally, researchers have attempted to calibrate the frequency response of probes through experiments to obtain more accurate static pressure fluctuation data [16–20]. However, these studies generally suffer from limitations such as a narrow range of applicability. Liu [21] generated broadband pulsating pressure signals using a signal generator and obtained the probe's transfer function in the time domain using parameters derived from a finite impulse response (FIR) adaptive filter. This method enabled the calibration of the probe's frequency response characteristics, with results showing good agreement with those obtained from reference sensors. Nevertheless, the study did not provide an in-depth analysis of the underlying mechanisms involved. Shalash [22] proposed using spectral analysis methods to calibrate pressure fluctuation data. Due to poor stability of the feedback function, this approach resulted in larger calibration errors. Boufidi [23] developed a theoretical model based on Helmholtz resonator theory, treating the model as a second-order system to estimate the frequency response characteristics of five-hole probes. Comparisons with experimental data revealed that the model could accurately predict characteristic frequencies but underestimated damping, leading to higher corrected static pressure fluctuation amplitudes. Joel [24] compared probe measurements with focused laser differential interferometry (FLDI) technology and found that calibrating probe pulsation pressure results using Helmholtz resonator theory was inaccurate, necessitating further corrections. Moriaux [25] attempted to use Bayesian functions to calibrate pressure fluctuation data, developing a semi-empirical method. However, the accuracy and applicability of this method remain unverified.

The resonance frequency of a Helmholtz resonator is derived from the wave equation. Panton [26] provided the formula for calculating the resonance frequency of a Helmholtz resonator. Chanaud [27] found that the geometric parameters of the Helmholtz resonator can lead to deviations from the resonance frequencies predicted by Panton's equation. Specifically, Panton's formula is most accurate for resonators with cubic geometries. Li [28] summarized the frequency response characteristics of Helmholtz resonators and concluded

that using the Helmholtz equation without correction factors often results in significant errors or even incorrect outcomes in many cases. It is recommended to adjust the parameters in the theoretical formula based on actual conditions, or to use numerical simulations to obtain more reliable predictions.

In this study, an interference-free pressure fluctuation environment was created using a standard sound source in an anechoic chamber. The frequency response characteristics of the fluctuating pressure sensor were measured both with and without the static pressure probe cavity. Through numerical simulations based on the Navier–Stokes equations, the frequency response characteristics of the static pressure probe cavity were investigated over a range from 500 Hz to 32 kHz. The impact of varying cavity dimensions on the frequency response of static pressure fluctuations was systematically analyzed. The time-domain results from numerical simulations were compared with those from the second-order system simulation, and the damping coefficient and characteristic frequency of the second-order system were obtained using the least squares method for fitting. The experimental, simulation, and second-order system frequency-domain data showed excellent agreement, elucidating the mechanism of the static pressure probe's frequency response. Based on these findings, a rapid calibration method for the frequency response of static pressure probes has been proposed.

2. Experimental Setup and Simulation Methods

2.1. Experimental Setup

As shown in Figure 1, single-frequency sine signals are produced by a signal generator. After being amplified by a power amplifier, these sine signals are emitted as sine waves by a speaker. Given that the sound waves are approximately plane waves and have sufficient amplitude intensity at a distance of 2 m from the speaker, the measurement apparatus and signal acquisition system are positioned 2 m away from the speaker. During the experiment, the following sensors and probes were used individually: a 15 Psi fluctuating pressure sensor, a 2 Psi fluctuating pressure sensor, a static pressure probe equipped with a 15 Psi fluctuating pressure sensor, a static pressure probe equipped with a 2 Psi fluctuating pressure sensor, and a microphone. Because of the absence of an incoming flow, the fluctuating pressure sensors can be directly exposed to the air. The fluctuating pressure measured under these conditions is considered the true static pressure fluctuation and is used for comparison with the static pressure fluctuation data obtained from the static pressure probe. To minimize interference from sound wave reflections, the experiment was conducted in an anechoic chamber, and the supports for the sensors and probes were wrapped with sound-absorbing glass wool.

The sound generation setup comprises an AWA1651 signal generator, an AWA5511B power amplifier, and an AWA5871 speaker, all provided by Aihua Instruments Company. The measurement setup employs Endevco 8507C-2 and 8507C-15 fluctuating pressure sensors, along with the corresponding acquisition systems. These sensors have dimensions of φ2.4 mm × 12.7 mm and a measurement accuracy better than 0.1%. The microphone used is a 1/2-inch B&K 4192 microphone, coupled with a B&K 4192 amplifier and a B&K 3050-A-040 data acquisition module. The data acquisition system employed a sampling frequency of 200 kHz. The experiment measured the response to single-frequency sinusoidal signals within a range from 500 Hz to 32 kHz, using one-third octave band frequencies.

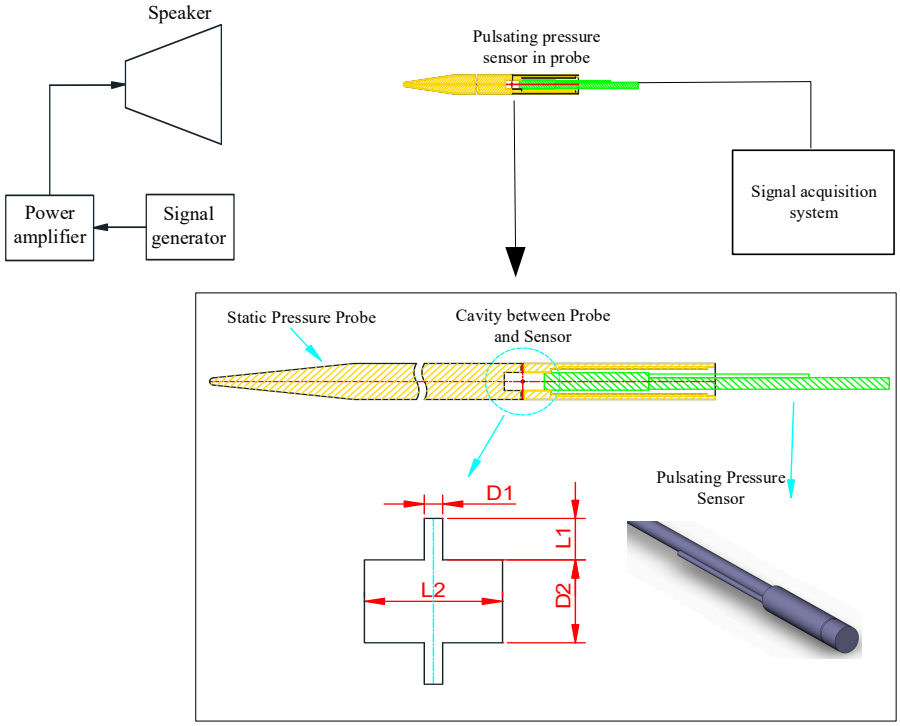

Figure 1. Schematic diagram of the experimental setup and probe cavity structure.

The static pressure probe is fabricated as shown in Figure 1. It features four static pressure taps arranged at 90° intervals, which are connected to the fluctuating pressure sensor through a cavity. The geometric parameters affecting the shape of the pressure taps and the cavity are defined as D1, D2, L1, and L2. For the static pressure probe used in the experiments, the parameters are D1 = 0.2 mm, L2 = 5 mm, L1 = 1.25 mm, and D2 = 2.5 mm.

2.2. Numerical Simulation Method

The numerical simulations are based on simplified control equations derived from the Navier–Stokes (N–S) equations. The N–S control equations are as follows:

$$\begin{aligned} &\frac{\partial \rho}{\partial t} + \nabla \cdot (\rho u) = 0 \\ &\frac{\partial (\rho u)}{\partial t} + \nabla \cdot (\rho u u^T) = \nabla \cdot \sigma + F \\ &\rho C_p \frac{\partial T}{\partial t} - \alpha_0 T \frac{\partial p}{\partial t} = -\nabla \cdot (q - u \cdot \tau) + Q \\ &\rho = \rho(p, T) \end{aligned} \tag{1}$$

The linear terms of the velocity perturbations are extracted, and the case of zero flow is considered:

$$\begin{aligned} &u(x,t) = u_0(x) + u(x)e^{i\omega t} \\ &u_0(x) = 0 \end{aligned} \tag{2}$$

By substituting into Equation (1), the resulting thermo-viscous acoustic equation can be expressed as:

$$\begin{aligned} &\frac{\partial \rho_t}{\partial t} + \nabla \cdot (\rho_0 u_t) = 0 \\ &\rho_0 \frac{\partial (u_t)}{\partial t} = \nabla \cdot \left[-p_t + \mu \left(\nabla u_t + (\nabla u_t)^T \right) - (\tfrac{2}{3}\mu - \mu_B)(\nabla \cdot u_t) \right] \\ &\rho_0 C_p \left(\frac{\partial T_t}{\partial t} + u_t \cdot \nabla T_0 \right) - \alpha_p T_0 \left(\frac{\partial p_t}{\partial t} + u_t \cdot \nabla p_0 \right) = -\nabla \cdot (k \nabla T_t) + Q \end{aligned} \tag{3}$$

In the numerical simulations, the source term Q is modeled as a sinusoidal signal.

As illustrated in Figure 2, the numerical model of the static pressure probe's cavity is configured with four narrow cylinders connected to a larger cylinder. A three-dimensional

structured mesh is utilized, to facilitate visualization, and the mesh is plotted by selecting every fifth grid point, with the mesh y+ value set to 0.12. The k-ω-SST (Shear Stress Transport) turbulence model is employed for this study. The time step size Δt for numerical simulations is determined based on the computational frequency, specifically $\Delta t = 1/(100f)$, ensuring that 100 steps are computed within each period of the signal. For the boundary conditions, the four small cylinders' inlets are specified as pressure inlets, receiving prescribed sinusoidal pressure fluctuation signals. All other boundaries are defined as no-slip adiabatic walls. In this setup, the choice of the k-ω-SST model is justified by its capability to accurately capture the near-wall turbulence characteristics, which is crucial for the current investigation. The selection of the time step ensures adequate resolution of the temporal variations of the flow field, while the boundary condition settings aim to simulate the physical phenomena as realistically as possible under the experimental constraints.

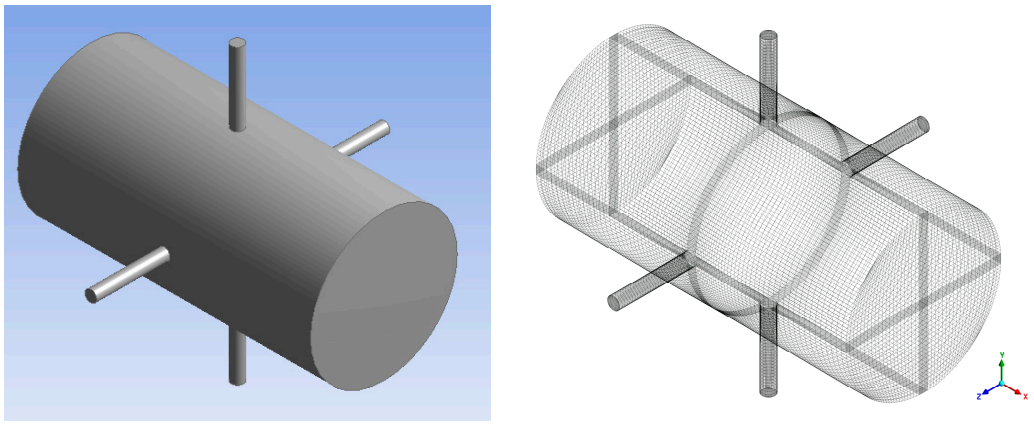

(**a**) (**b**)

Figure 2. Numerical simulation model and mesh for the static pressure probe cavity. (**a**) Numerical simulation model; (**b**) numerical simulation mesh (the display updates every four grid cells).

The pressure fluctuations at the end face of the larger cylinder are monitored. As detailed in Table 1, seven distinct cavity geometries are simulated to examine the influence of cavity geometry on the frequency response characteristics of static pressure fluctuations.

Table 1. Numerical simulation of different parameter conditions for the cavity.

	L1 (mm)	L2 (mm)	D1 (mm)	D2 (mm)
Condition 1	1.25	5	0.1	1.25
Condition 2	1.25	5	0.3	1.25
Condition 3	1.25	5	0.2	1.25
Condition 4	1.25	5	0.2	1.5
Condition 5	1.25	5	0.2	2.5
Condition 6	1.25	2.5	0.2	5
Condition 7	1.25	4	0.2	1.25

2.3. Second-Order System Simulation Method

We found that the frequency response characteristics of the static pressure probe's pulsating pressure are similar to those of a second-order system. Therefore, a second-order system is employed to model the oscillation of the compressible air within the cavity to verify whether the cavity's influence on the frequency response of the static pressure probe adheres to the second-order system mechanism. Assuming the static pressure probe's

cavity and sensor form a damped second-order linear system, the transfer function is formulated as follows:

$$G(s) = \frac{w_0^2}{s^2 + 2\xi w_0 s + w_0^2} \tag{4}$$

In the transfer function, w_0 is the natural frequency of the system, and ξ is the damping ratio.

This transfer function is employed to analyze the frequency response characteristics of the static pressure probe and to understand the impact of the cavity geometry on the system's behavior. When $\xi > 1$, the system is overdamped. If the input signal frequency matches the characteristic frequency of the system, the pulsating pressure signal is attenuated by the cavity system. Conversely, when $\xi < 1$, the system is underdamped. When the input signal frequency matches the characteristic frequency of the system, the pulsating pressure signal is amplified by the cavity system. In this case, if the input signal frequency is less than the characteristic frequency, the amplification factor of the pulsating pressure signal increases with increasing frequency. When $\xi = 1$, the system is critically damped, and the cavity system has no effect on the pulsating pressure signal. The frequency response characteristic of a second-order linear system is given by the following formula:

$$\begin{aligned} |A(w)| = |G(jw)| &= \left| \frac{w_0^2}{(jw)^2 + 2\xi w_0 jw + w_0^2} \right| \\ &= \frac{w_0^2}{\sqrt{\left(w_0^2 - w^2\right)^2 + (2\xi w_0 w)^2}} \end{aligned} \tag{5}$$

Converting the angular frequency to linear frequency, we obtain the following:

$$|A(f/f_0)| = \frac{1}{\sqrt{\left[1 - (f/f_0)^2\right]^2 + 4\xi^2 (f/f_0)^2}} \tag{6}$$

For a second-order linear system, when a step input is applied, it can be understood from the Fourier transform that the step signal can be considered as the superposition of an infinite number of sinusoidal signals. The function is defined as follows:

$$Z(f, \xi^2) = |A(f/f_0)| \tag{7}$$

The characteristic frequency of the cavity system is determined by fitting the data using the least squares method, as follows:

$$\frac{d\sum_i \left[Z(f_i, \xi^2) - Z_i\right]^2}{d\xi^2} = 0 \tag{8}$$

The verification process for a damped second-order linear system, as well as the numerical simulation process, is illustrated in Figure 3. Both methods entail dividing the computed output signal by the input signal to determine the amplification factor. The key difference lies in the fact that the numerical simulation requires setting different frequencies of sinusoidal input signals, whereas the second-order linear system can perform the sweep calculation with a step input signal.

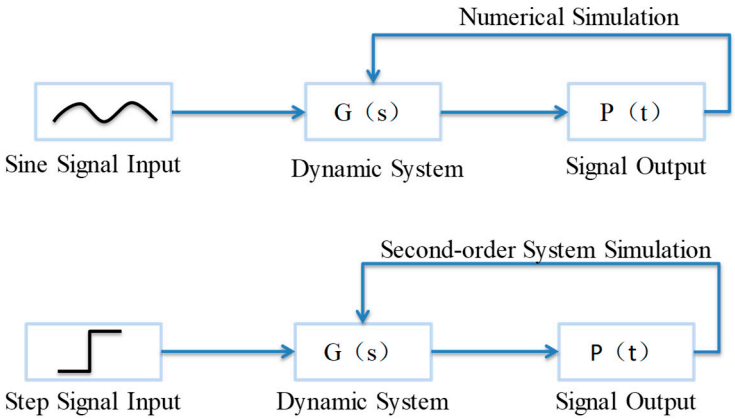

Figure 3. Verification of second-order linear system simulation and comparison of numerical simulation procedures.

3. Results and Discussion

3.1. Experimental Results and Analysis

Sine input signals with different frequencies were provided in a range from 500 Hz to 32 kHz, spaced at one-third octave intervals. First, the frequency response characteristics of the fluctuating pressure sensors were investigated. Figure 4 shows the time-domain response curves of the 15 Psi and 2 Psi fluctuating pressure sensors for 2 kHz and 8 kHz sine input signals. It can be observed that at lower frequencies, the pressure curve measured by the 15 Psi fluctuating pressure sensor is less smooth compared to that of the 2 Psi fluctuating pressure sensor. However, when the input signal frequency increases to 8 kHz, the time-domain response characteristics of the two sensors become very similar.

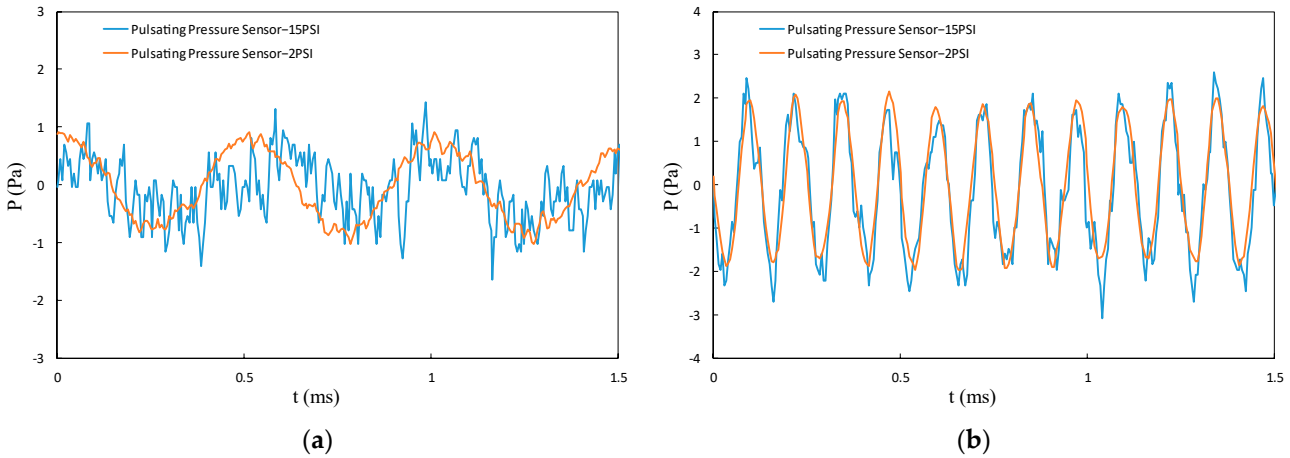

Figure 4. Comparison of time-domain response curves of 15 Psi and 2 Psi pulsating pressure sensors under different frequency sine input signals. (**a**) Time-domain response comparison at 2 kHz sine input signal; (**b**) time-domain response comparison at 8 kHz sine input signal.

Figure 5 shows the root mean square (RMS) values of the fluctuating pressure (noise intensity) measured by the 15 Psi and 2 Psi fluctuating pressure sensors and the microphone when they are not installed inside the static pressure probe. It can be observed that the three measurements exhibit good consistency. The noise intensity measured by the 2 Psi sensor falls within the middle region of the error band, indicating higher reliability. Therefore, the 2 Psi fluctuating pressure sensor is selected for measuring static pressure fluctuations in the static pressure probe.

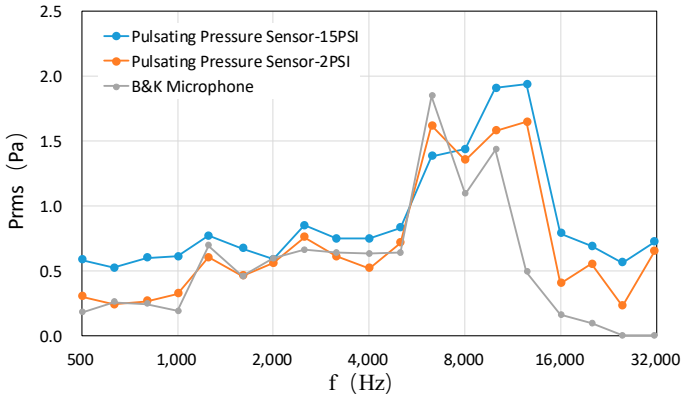

Figure 5. Fluctuating pressure measured by 15 Psi and 2 Psi sensors and a microphone at different frequencies.

Due to the non-linear deformation of the speaker diaphragm at high power levels, the signal generation system imposes a limit on the power amplifier. The speaker can generate a maximum sine wave signal of approximately 100 dB while ensuring no signal distortion. To achieve more accurate measurement results, the signal input system operates at near full power during the experiments. To verify the stability of the sound source and measurement systems, repeatability tests were conducted using the 2 Psi fluctuating pressure sensor without the static pressure probe. The test results are presented in Figure 6. It can be observed that the test results exhibit good consistency, with the overall system error being less than 5%.

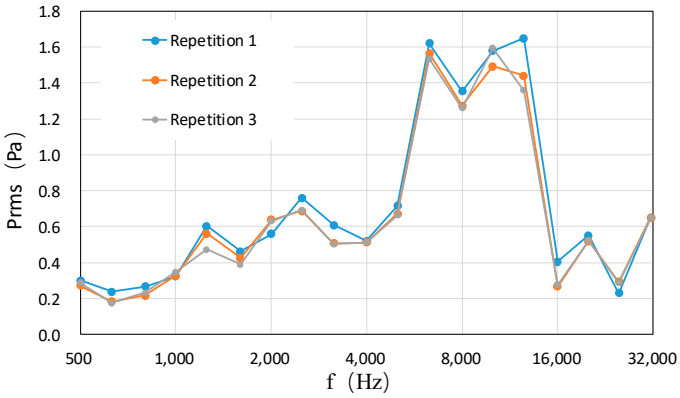

Figure 6. Repeatability of measurement results from the 2 Psi fluctuating pressure sensor.

Figure 7 illustrates the pressure oscillations measured by the fluctuating pressure sensor at different frequencies, both with and without the static pressure probe. The internal pressure tap and cavity parameters of the static pressure probe are D1 = 0.2 mm, L2 = 5 mm, L1 = 1.25 mm, and D2 = 2.5 mm, as shown in Figure 1. From Figure 7, it can be observed that the highest-pressure oscillation occurs at 6300 Hz without the static pressure probe. However, when the fluctuating pressure sensor is installed inside the static pressure probe, the internal cavity modifies the frequency response characteristics. In this case, the highest-pressure oscillation occurs in the vicinity of 3000 Hz, and the peak pressure fluctuation at 6300 Hz is significantly reduced.

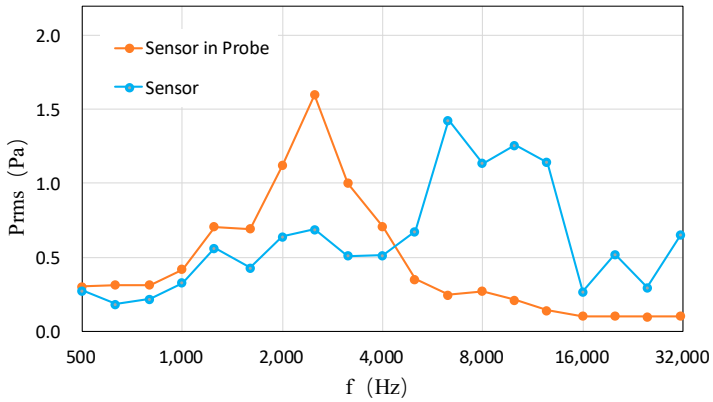

Figure 7. Fluctuating pressure measured by the sensors inside and outside the static pressure probe.

The cavity structure of the static pressure probe significantly affects the amplitude-frequency response characteristics of the pressure fluctuations. By dividing the measurement results of the fluctuating pressure sensor inside the static pressure probe by the results obtained without the static pressure probe, the amplification factor of the static pressure probe at different frequencies can be determined. The characteristic frequency of the amplification factor is related to the internal cavity structure of the static pressure probe. The experimentally measured amplification factors will be presented in subsequent sections of this paper, along with comparisons to numerical simulations.

3.2. Numerical Simulation Results and Analysis

Numerical simulations were performed to calculate the amplification factor of the static pressure probe under the same operating conditions as the experimental measurements. Specifically, the internal pressure tap and cavity parameters of the static pressure probe were set to D1 = 0.2 mm, L2 = 5 mm, L1 = 1.25 mm, and D2 = 2.5 mm. The amplification factor is defined as the ratio of the root mean square (RMS) value of the pressure fluctuations measured by the sensor when installed inside the probe to the RMS value of the pressure fluctuations measured by the sensor when it is directly exposed to the air.

Figure 8a illustrates the comparison between the experimental and numerical simulation results for the amplification factor of the static pressure probe. It is evident that the numerical simulation results closely match the experimental data, with both exhibiting the same characteristic frequency. Minor discrepancies between the experimental and numerical results can be attributed to experimental errors. Notably, the amplification factor at the characteristic frequency in the experimental results is marginally lower than that obtained from the numerical simulations. This slight difference is likely due to minor disturbances inherent in the experimental setup, which may hinder the continuous increase in amplitude at the characteristic frequency.

Figure 8b shows the pressure distribution contour within the static pressure probe at the characteristic frequency. It can be observed that the pressure fluctuations increase significantly within the pressure tap, while the increase is relatively gradual within the larger cavity. This indicates that the pressure tap of the static pressure probe significantly influences the frequency response and its geometric parameters (D1, L1) are of particular importance.

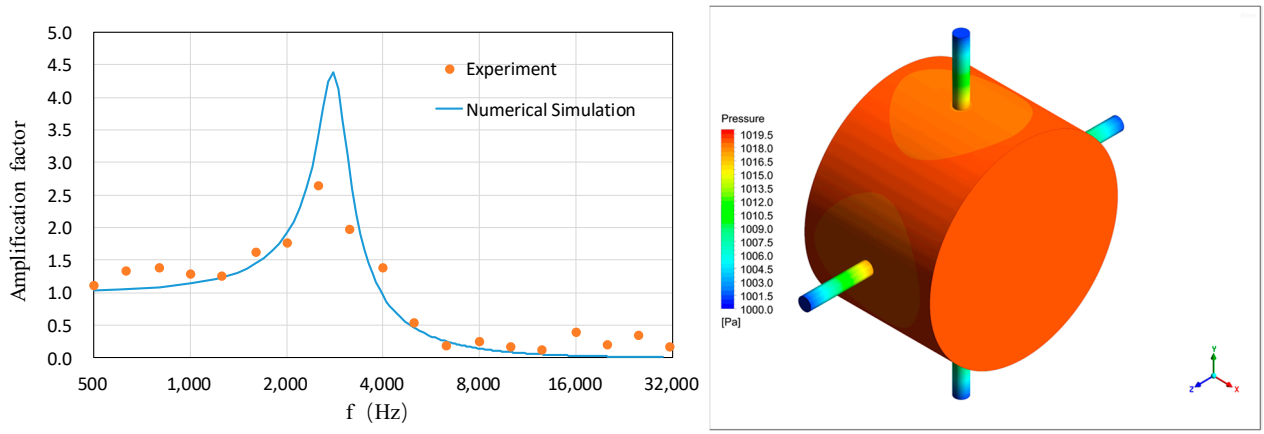

Figure 8. Comparison of experimental results and numerical simulation results for the amplification coefficient of fluctuating pressure in the static pressure probe. (**a**) Comparison of frequency response results; (**b**) numerical simulation pressure contour at characteristic frequency.

After verifying the good agreement between the numerical simulations and the experimental results, the numerical simulation system was employed to investigate the influence of the geometric parameters of the pressure tap and cavity on the amplification factor. The geometric parameters include the diameter of the pressure tap (D1), the depth of the pressure tap (L1), the diameter of the cavity (D2), and the height of the cavity (L2). Table 1 presents seven typical calculation conditions, and additional conditions were also explored. Figure 9 illustrates the effects of different pressure tap and cavity geometric parameters on the amplitude-frequency and phase-frequency responses of the static pressure probe.

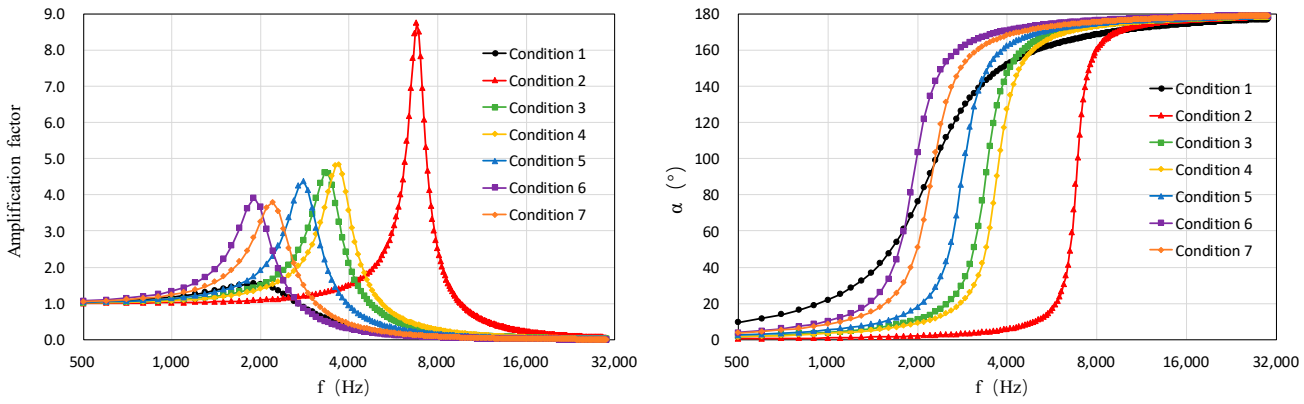

Figure 9. Frequency response curves of the static pressure probe's pressure tap and cavity under different geometric parameter conditions. (**a**) Comparison of amplitude-frequency response; (**b**) comparison of phase-frequency response.

From Figure 9a, it can be observed that all four geometric parameters of the cavity (D1, L1, D2, L2) affect the characteristic frequency of the pressure fluctuation amplification factor of the static pressure probe. The results indicate that the diameter of the pressure tap (D1) is the most significant parameter influencing the magnitude of the amplification factor. Specifically, when D1 is 0.1 mm, the amplification factor is only 1.4, whereas when D1 increases to 0.3 mm, the amplification factor rises to 8.9. In comparison, the other parameters (L1, D2, L2) have a lesser impact on the magnitude of the amplification factor.

From Figure 9b, it can be observed that the pressure fluctuations in the static pressure probe experience a phase inversion (a phase shift of 180°) at the characteristic frequency of the cavity. The rate of this phase inversion is proportional to the amplification factor.

Figure 10 illustrates the trends of dimensionless cavity geometric parameters on the amplification factor of the static pressure probe at the characteristic frequency. It can be observed that as the diameter of the pressure tap (D1) increases, the amplification factor at the characteristic frequency rises rapidly. Conversely, as the depth of the pressure tap (L1), the diameter of the cavity (D2), and the volume of the cavity (V) increase, the amplification factor at the characteristic frequency decreases gradually, with the rate of change being much smaller compared to that caused by the diameter of the pressure tap (D1).

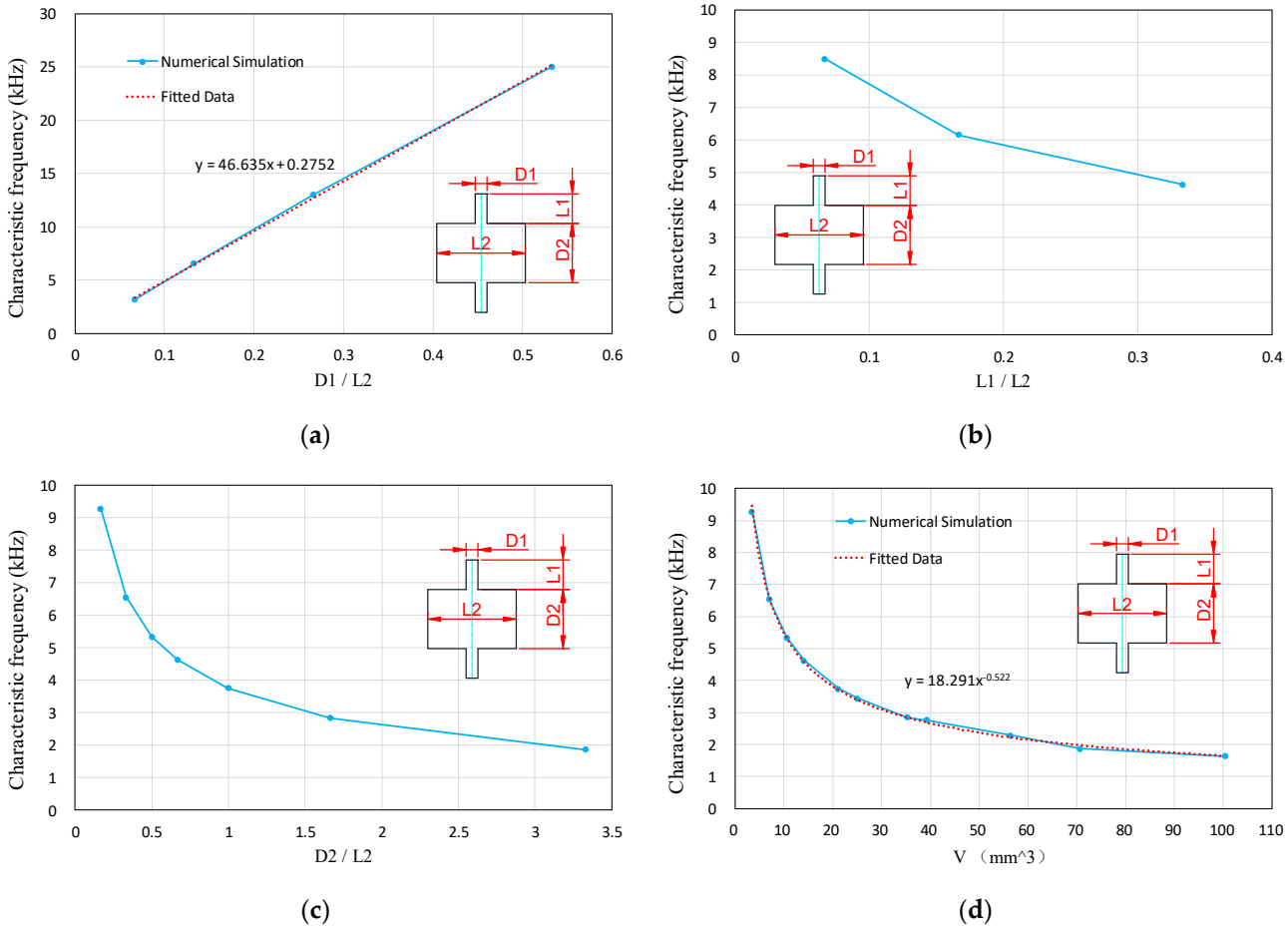

Figure 10. Influence of different geometric parameters of the static pressure probe cavity on the amplification coefficient of fluctuating pressure at characteristic frequencies. (**a**) Effect of pressure tap diameter on the amplification coefficient; (**b**) effect of pressure tap depth on the amplification coefficient; (**c**) effect of cavity depth on the amplification coefficient; (**d**) effect of cavity volume on the amplification coefficient.

According to the numerical simulation results, it is evident that by selecting an appropriate diameter for the pressure tap, the amplification factor of the pressure fluctuations in the static pressure probe can be adjusted to be close to one. In this case, the static pressure fluctuation data are reliable for measurement frequencies below the characteristic frequency of the cavity. Additionally, by adjusting the depth of the pressure tap (L1), the diameter of the cavity (D2), and the height of the cavity (L2) to increase the characteristic frequency of the cavity, accurate static pressure fluctuation measurements can be achieved over a wider frequency range.

The classical formula for the resonance frequency of a Helmholtz resonator is given below:

$$f = \frac{c}{2\pi}\sqrt{\frac{S}{VL}} \tag{9}$$

In the equation, c is the local speed of sound, S is the area of the orifice, V is the volume of the cavity, and L is the depth of the orifice.

Numerical simulation results show that the influence of the probe cavity's geometric parameters on the characteristic frequency follows the same pattern as described by the Helmholtz resonance equation. Specifically, the diameter of the pressure tap exhibits a linear relationship with the characteristic frequency, whereas the cavity volume has an inverse square root (-0.5 power) relationship with the characteristic frequency. Referring to the Helmholtz resonance equation, a semi-empirical formula was developed to predict the characteristic frequency of the static pressure probe cavity, as follows:

$$f = \frac{c}{2\pi}\sqrt{\frac{4S}{V(L1+2D1)}} = \frac{c}{\pi}\sqrt{\frac{D1^2}{D2^2L2(L1+2D1)}} \tag{10}$$

In the equation, S is the area of a single pressure tap; as there are four pressure taps, the total area is 4S. V is the volume of the cavity, consistent with the Helmholtz resonance equation. The term (L1 + 2D1) represents a correction factor applied to the Helmholtz equation.

3.3. Second-Order System Simulation Results and Analysis

The frequency response characteristics of the static pressure probe cavity were calculated using a second-order system model. To facilitate a direct comparison, the geometric parameters of the cavity were set to be identical to those utilized in the experimental measurements, specifically, D1 = 0.2 mm, L2 = 5 mm, L1 = 1.25 mm, and D2 = 2.5 mm. According to Equation (8), 50 points per period were extracted from the time-domain data of the numerical simulation results at a specific frequency. The differences between these 50 points' time and pressure amplitude values and those of the second-order system were summed, and the damping coefficient and characteristic frequency of the second-order system were determined using the least squares method.

It was found that for a static pressure probe with cavity geometric parameters D1 = 0.2 mm, L2 = 5 mm, L1 = 1.25 mm, and D2 = 2.5 mm, the error between the second-order system and the simulation and numerical simulation results was minimized when the damping coefficient was 0.084 and the characteristic frequency was 2.94 kHz. Figure 11a compares the time-domain data of the second-order system and numerical simulations at a damping coefficient of 0.084 and a characteristic frequency of 2.94 kHz. Figure 11b contrasts the frequency-domain characteristics of the second-order system, numerical simulations, and experimental results under the same conditions. It can be observed that both the time-domain and frequency-domain results show excellent agreement.

From the comparison, it is evident that the cavity behaves as a second-order underdamped system. This system first amplifies and then attenuates the pressure fluctuations measured by the pressure tap of the static pressure probe over the frequency range, with the maximum amplification occurring at the characteristic frequency of the cavity. The compressibility of the air within the cavity means that the fundamental nature of the system as a second-order underdamped system cannot be altered. However, the damping of the second-order system can be adjusted by modifying the geometric parameters of the cavity to approach a value of one. This ensures that the static pressure fluctuations measured by the static pressure probe are relatively accurate across the frequency spectrum.

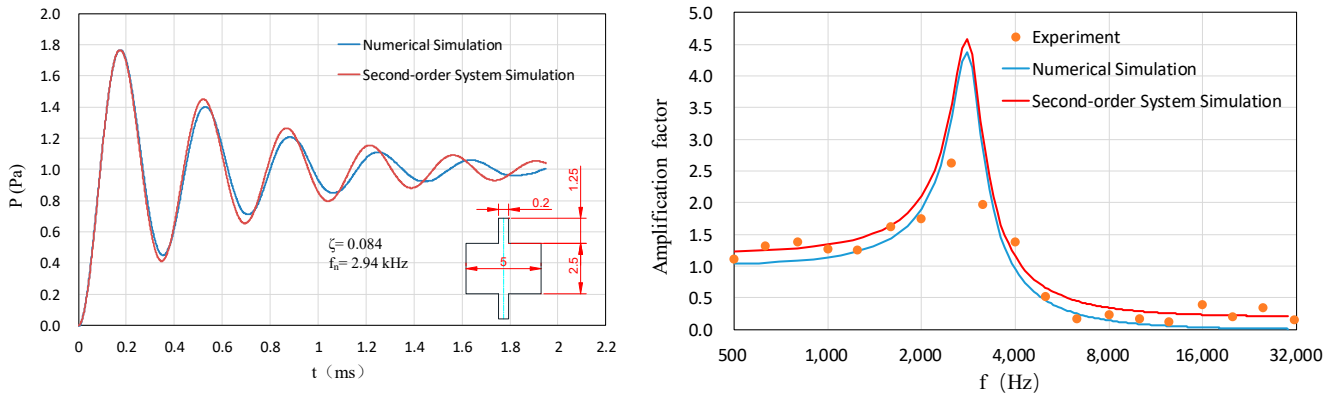

Figure 11. Comparison of second-order system simulation and numerical simulation results. (**a**) Time-domain results; (**b**) frequency-domain results.

Based on the aforementioned research results, there is a high degree of consistency between experimental data, numerical simulations, and second-order system simulations. This finding provides a rapid method for calibrating the frequency response characteristics of static pressure probe cavities. Specifically, this method involves using numerical simulations to calculate the cavity response at a specific frequency and fitting the time-domain parameters (time and amplitude) from the numerical simulation results to a second-order system model. By obtaining the damping coefficient and frequency of the second-order system, the transfer function of the second-order system can be used to quickly calibrate the frequency response data of the static pressure probe cavity across all frequencies. Compared to performing scan-based numerical simulations over the entire frequency band, this approach significantly reduces computational time. Additionally, it addresses the issue of inaccurate damping predictions that arise when using only theoretical models, as noted by Boufidi [23]. Through this method, the frequency response characteristics of static pressure probes can be rapidly corrected, yielding accurate static pressure fluctuation results.

4. Conclusions

In this study, we experimentally compared the frequency domain response of fluctuating pressures measured with and without a static pressure probe. Numerical simulations were conducted to explore the impact of the geometric parameters of the static pressure probe's cavity structure on the measurement of fluctuating pressure. By modeling the cavity structure as a second-order system, we elucidated the mechanisms influencing the frequency response characteristics of the static pressure probe. Additionally, we fitted a semi-empirical formula to predict the characteristic frequency of fluctuating pressure for static pressure probes and proposed a rapid calibration method for fluctuating pressure measurements. The primary findings are summarized as follows:

1. The internal cavity of the static pressure probe functions as a second-order underdamped system, modifying the frequency response of the fluctuating pressure detected by the pressure tap. Below the cavity's characteristic frequency, the fluctuating pressure signal is amplified as frequency increases. Conversely, above the characteristic frequency, the phase of the fluctuating pressure shifts by 180°, and its amplitude diminishes with increasing frequency.
2. The frequency response characteristics of the static pressure probe cavity resemble those of a Helmholtz resonator, where geometric parameters of the cavity can alter both the characteristic frequency and amplitude of the amplification factor. Among these parameters, the diameter of the pressure tap is the most significant. Through

the semi-empirical formula developed in this study, the characteristic frequency of the static pressure probe cavity can be accurately predicted.

3. By optimizing the geometric parameters of the cavity, it is possible to adjust the amplification factor at the characteristic frequency to approach one, where the system's damping coefficient is also near one, and to maximize the characteristic frequency. This ensures that fluctuating pressure signals below the cavity's characteristic frequency are measured with greater accuracy.
4. Based on the mechanism that the cavity behaves as a second-order underdamped system, the transfer function of the second-order system can be derived from numerical simulation results at a single frequency. This enables the rapid correction of fluctuating pressure signals across all frequencies measured by the static pressure probe, thereby obtaining accurate fluctuating pressure data.

Author Contributions: C.W.: conceptualization, methodology, software, writing—original draft, writing—review and editing, funding acquisition. X.Y.: formal analysis, methodology, writing—original draft. J.L.: investigation, resources, writing—review and editing. Q.P.: writing—original draft, writing—review and editing, project administration, funding acquisition. All authors have read and agreed to the published version of the manuscript.

Funding: This work is supported by the fund of Technology Research (2200070019).

Data Availability Statement: The datasets analyzed during the current study are available from the corresponding authors on reasonable request.

Conflicts of Interest: The authors declare no conflicts of interest.

References

1. Fedorov, A. Transition and stability of high-speed boundary layers. *Annu. Rev. Fluid Mech.* **2011**, *43*, 79–95. [CrossRef]
2. Schneider, S.P. Developing mechanism-based methods for estimating hypersonic boundary-layer transition in flight: The role of quiet tunnels. *Prog. Aerosp. Sci.* **2015**, *72*, 17–29. [CrossRef]
3. Hoffman, E.N.; Kendhammer, D.M.; LaLonde, E.J.; Andrade, A.; Combs, C.S. Effects of distributed roughness on shock-wave/boundary-layer interactions at Mach 7.2. In Proceedings of the AIAA SCITECH 2023 Forum, National Harbor, MD, USA, 23–27 January 2023; p. 0268.
4. Wendt, V.; Simen, M.; Hanifi, A. An experimental and theoretical investigation of instabilities in hypersonic flat plate boundary layer flow. *Phys. Fluids* **1995**, *7*, 877–887. [CrossRef]
5. Bounitch, A.; Lewis, D.; Lafferty, J. Improved measurements of "Tunnel Noise" pressure fluctuations in the AEDC hypervelocity wind tunnel No. 9. In Proceedings of the 49th AIAA Aerospace Sciences Meeting including the New Horizons Forum and Aerospace Exposition, Orlando, FL, USA, 4–7 January 2011; p. 1200.
6. Mai, C.L.; Bowersox, R.D. Effect of a normal shock wave on freestream total pressure fluctuations in a low-density Mach 6 flow. In Proceedings of the 44th AIAA Fluid Dynamics Conference, Atlanta, GA, USA, 16–20 June 2014; p. 2641.
7. Ananthapadmanaban, R.; McIntyre, T.J.; Wheatley, V.; Mee, D.J. Noise generated in a scramjet combustor. In Proceedings of the AIAA SCITECH 2023 Forum, National Harbor, MD, USA, 23–27 January 2023. [CrossRef]
8. Donovan, F.M., Jr.; Taylor, B.C.; Su, M.C. One-dimensional computer analysis of oscillatory flow in rigid tubes. *J. Biomech. Eng.* **1991**, *113*, 476–484. [CrossRef]
9. Aydin, I. Evaluation of fluctuating pressures measured with connection tubes. *J. Hydraul. Eng.* **1998**, *124*, 413–418. [CrossRef]
10. Liu, X.; Yi, S. Experimental investigation about the aerodynamic noise caused by hypersonic turbulence. *Phys. Fluids* **2024**, *36*, 016101. [CrossRef]
11. Shirahama, Y. Development of the probe to measure static-pressure fluctuations. *Trans. Jpn. Soc. Mech. Eng.* **1993**, *567*, 79–85.
12. Toyoda, K.; Okamoto, T.; Shirahama, Y. Eduction of vortical structures by pressure measurements in noncircular jets. *Appl. Sci. Res.* **1994**, *53*, 237–248. [CrossRef]
13. Kawata, T.; Maeda, H.; Obi, S. An attempt to measure fluctuating local pressure in free turbulent flow in water. *J. Fluid Sci. Technol.* **2014**, *9*, JFST0014. [CrossRef]
14. Kawata, T.; Naka, Y.; Fukagata, K.; Obi, S. Simultaneous measurement of velocity and fluctuating pressure in a turbulent wing-tip vortex using triple hot-film sensor and miniature total pressure probe. *Flow Turbul. Combust.* **2011**, *86*, 419–437. [CrossRef]

15. Chaudhry, R.S.; Candler, G.V. Recovery of freestream acoustic disturbances from stagnation pressure spectrum in hypersonic flow. In Proceedings of the 54th AIAA Aerospace Sciences Meeting, San Diego, CA, USA, 4–8 January 2016; p. 2059.
16. Pereira, J.D. Pressure Sensors: Working Principles of Static and Dynamic Calibration. *Sensors* **2024**, *24*, 629. [CrossRef] [PubMed]
17. Yu, Z.; Hong-yan, Z.; Jing, Z.; Dong-xing, P. The Dynamic Calibration Method of High-Pressure Transducer under High-Static Pressure. In Proceedings of the 2011 International Conference on Mechatronic Science, Electric Engineering and Computer (MEC), Jilin, China, 19–22 August 2011.
18. Wu, G.; Guo, X.; Yang, K.; Yang, H. A robust calibration method for seven-hole pressure probes. *Exp. Fluids* **2019**, *60*, 120. [CrossRef]
19. Pfau, A.; Schlienger, J.; Kalfas, A.; Abhari, R.S. Virtual four sensor fast response aerodynamic probe (FRAP®). *E3S Web Conf.* **2022**, *345*, 01014. [CrossRef]
20. Zhang, F.; Liu, D.; Liu, A.; Gang, X.; Li, L. Numerical study on the phase sensitivity variation in low frequency primary microphone calibrations. *Appl. Sci.* **2020**, *10*, 3799. [CrossRef]
21. Liu, F.; Cai, X.; Cai, T. Inverse transfer function identification for high-frequency pressure probes using M-sequence pressure generators. *Flow Meas. Instrum.* **2022**, *87*, 102221. [CrossRef]
22. Shalash, K.; Şahin, F.C.; Schiffmann, J. Non-linear transfer function identification of pressure probes using Siren Disks. *Exp. Therm. Fluid Sci.* **2018**, *91*, 459–469. [CrossRef]
23. Boufidi, E.; Alati, M.; Fontaneto, F.; Lavagnoli, S. Design and testing of a miniaturized five-hole fast response pressure probe with large frequency bandwidth and high angular sensitivity. *J. Eng. Gas Turbines Power* **2019**, *141*, 101010. [CrossRef]
24. Lawson, J.M.; Neet, M.C.; Hofferth, J.W.; Austin, J.M. Supersonic freestream density fluctuations from focused laser differential interferometry and pitot-probe measurements. *AIAA J.* **2022**, *60*, 5173–5186. [CrossRef]
25. Moriaux, O.K.; Zamponi, R.; Schram, C.F. Development of a model-driven calibration method for remote microphone probes using Bayesian inference. In Proceedings of the AIAA AVIATION 2023 Forum, San Diego, CA, USA, 12–16 June 2023; p. 4059.
26. Panton, R.L.; Miller, J.M. Resonant frequencies of cylindrical Helmholtz resonators. *J. Acoust. Soc. Am.* **1975**, *57*, 1533–1535. [CrossRef]
27. Chanaud, R.C. Effects of geometry on the resonance frequency of Helmholtz resonators. *J. Sound Vib.* **1994**, *178*, 337–348. [CrossRef]
28. Li, L.; Liu, Y.; Zhang, F.; Sun, Z. Several explanations on the theoretical formula of Helmholtz resonator. *Adv. Eng. Softw.* **2017**, *114*, 361–371. [CrossRef]